8-31-1998

Bound State Semiclassical Wave Functions

Stephen Knudson

J. B. Delos
William & Mary, jbdelo@wm.edu

D. W. Noid

Recommended Citation

Knudson, Stephen; Delos, J. B.; and Noid, D. W., Bound State Semiclassical Wave Functions (1998). *Journal of Chemical Physics*, 84(12).
10.1063/1.450693

Bound state semiclassical wave functions

S. K. Knudson
Department of Chemistry, College of William and Mary, Williamsburg, Virginia 23185
J. B. Delos
Department of Physics, College of William and Mary, Williamsburg, Virginia 23185
D. W. Noid[a)]
Chemistry Division, Oak Ridge National Laboratories, Oak Ridge, Tennessee 37830

(Received 8 January 1986; accepted 4 March 1986)

The semiclassical theory developed by Maslov and Fedoriuk is used to calculate the wave function for a two-dimensional bound state system. We investigate in detail an eigenstate of a coupled anharmonic oscillator system. The primitive semiclassical wave function is obtained from the characteristic function S and the density function J. Each of these functions consists of four branches corresponding to the four possible directions of motion of the classical trajectory through any point. The interference from the four branches determines the basic structure of the wave function. A uniform approximation gives a wave function which is well behaved along each caustic and which is in good agreement with the fully quantal wave function.

I. INTRODUCTION

In this paper we find a semiclassical wave function for a two-dimensional bound state system using the method of Maslov and Fedoriuk.[1] This method was discussed by one of us in an earlier paper (denoted I) and subsequently used to calculate a wave function for a scattering system.[2] We follow the notation of those papers, and include only enough detail here to make this paper reasonably self-contained. The purpose is to show the application of the method to a bound state system, emphasizing similarities with and differences from the scattering case previously considered.[2] We begin by reviewing the method, which is based on the mathematical analysis of Maslov, and apply it to the present model system. We then examine closely the resulting wave function for one of the states of a two-dimensional anharmonic oscillator.[3]

The objective is to determine the semiclassical approximation to the wave function which is the solution of the Schrödinger equation

$$[H(-i\hbar\partial/\partial q,q)-E]\Psi(q)=0, \tag{1.1}$$

where q denotes the set of configuration space variables, which for the system considered here are the Cartesian coordinates (x,z). The classical Hamiltonian function $H(p,q)$ associated with the operator $H(-i\hbar\partial/\partial q,q)$ is defined in a four-dimensional phase space $(p,q)=(p_x,p_z,x,z)$. In particular, we consider here a bound state of a system described by the classical coupled anharmonic oscillator Hamiltonian

$$\begin{aligned} &H(p,q)=T+V,\\ &T=(p_x^2+p_z^2)/(2M),\\ &V=k_x x^2+k_z z^2+k_{12}xz^2+k_{30}x^3, \end{aligned} \tag{1.2}$$

where M is the mass of the particle and k's are the force constants and coupling constants. We take $\hbar=1, M=1, k_x=0.49$, $k_z=1.69$, $k_{12}=-0.1$, and $k_{30}=-0.01$, in agreement with several previous studies.[4]

[a)] Research sponsored by the U.S. Department of Energy under contract DE-AC05-840R21400 with Martin Marietta Energy Systems, Inc.

II. THE TRAJECTORY AND ITS ASSOCIATED FUNCTIONS

A. Classical trajectory

The first step in finding the semiclassical wave function is to determine the "eigentrajectory." A trajectory is calculated by integration of Hamilton's equations of motion

$$dp_i/dt=-\partial H/\partial q_i;\quad dq_i/dt=\partial H/\partial p_i,\quad i=x,z. \tag{2.1}$$

Simultaneously, the characteristic function $S(t)$ is calculated by integration of the differential equation

$$dS(t)/dt=p\cdot dq/dt=\sum_i p_i(t)dq_i(t)/dt. \tag{2.2}$$

The initial values p^0, q^0 must satisfy both (i) a fixed energy condition

$$H(p^0,q^0)=E \tag{2.3}$$

and (ii) a restriction on the characteristic function $S^0(q^0)$:

$$dS^0=p^0\cdot dq^0. \tag{2.4}$$

Other than this, the initial conditions are arbitrary, and are chosen to obtain an eigentrajectory satisfying the two semiclassical EBK[5] quantum conditions:

$$A_i=\oint p\cdot dq=(n_i+1/2)2\pi,\quad i=1,2, \tag{2.5}$$

where n_1 corresponds roughly to an x quantum number, n_2, a z quantum number. The quantum conditions can be applied easily when the motion is quasiperiodic, because such a trajectory occupies a limited portion of configuration space bounded by caustics. To impose these conditions, we generate the surface of section at $x=0$ to obtain A_2, and use S to determine the total phase around a loop, giving A_1+A_2; details of this procedure are given in Ref. 6. We started the trajectories at $x^0=0, z^0=0$, and varied p_x^0 and p_z^0 in a systematic search until the appropriate values of A_i were obtained. Once the initial conditions for the eigentrajectory have been found, the trajectory integration generates

 0021-9606/86/126886-09$02.10

(pointwise) the functions $x(t), z(t), p_x(t), p_z(t)$, and $S(t)$.

We consider here the state with $n_1 = 6$ and $n_2 = 3$, for which we found the energy to be 8.651 43. This is the 46th state, but the 20th state of odd parity. (For comparison, the energy obtained from a fully quantum mechanical variational calculation using a 300 state harmonic oscillator basis is 8.651 295.) Figure 1 shows a plot of the trajectory, which is evidently quasiperiodic; the caustics are also drawn in the figure.

B. The Lagrangian manifold

The functions $[p(t), q(t)]$ form a two-dimensional surface in phase space, called a Lagrangian manifold. The manifold can be separated into a number of overlapping domains, each of which uses two phase space coordinates as the appropriate variables for the domain. A *regular* domain has a smooth and smoothly invertible projection into some portion of configuration space. Then the coordinates x and z can be regarded as independent variables, and the embedding of the manifold in the phase space can be described by the smooth functions $p_x(x,z)$ and $p_z(x,z)$.

There are four different sets of values of (p_x,p_z) associated with any point (x,z), leading to the existence of four sheets of the manifold. Figure 2 shows two of the four sheets, by plotting $p_z = p_z(x,z)$. We label the sheets by recognizing that for either $|x|$ or $|z|$ not too large, the direction of motion of the trajectory, as given by the four possible sign combinations of the two momenta, can serve to determine the sheet on which the trajectory lies at time t. (For large $|x|$ and large $|z|$, a different rule for this assignment is needed, and will be given below.) The numbering of the sheets is specified in Table I.

Not all domains of the manifold are regular. Singular points on the manifold are defined as those points which project onto the caustics in configuration space, and any domain containing a singular point is singular (not regular). The regular domains (1–4) of the manifold are defined as those portions of the corresponding sheets which are sufficiently far from the singular points. For the singular domains, there is no smoothly invertible projection into configuration space, and an alternative set of variables must be used. Lagrangian manifolds have the property that it is always possible to pick a set of coordinates and momenta (p_α,q_β) containing no canonically conjugate pairs, such that the projection from the manifold to the selected variables is smooth and smoothly invertible. Near the upper and lower caustics (large $|z|$–see Fig. 1) the appropriate selection of independent variables is (x,p_z), while near the right or left caustics (large $|x|$) it is (p_x,z). Each of the singular regions corresponding to a caustic is thus defined to be a separate domain of the manifold, overlapping with regular domains. In addition, each of the regions which projects close to a corner, where two caustics intersect, is also taken to be a separate domain, with (p_x,p_z) as the variables. Thus as the trajectory evolves in time it passes from one regular domain to another, glancing off at least one caustic in configuration space and passing through at least one singular domain of the manifold as it does so.

The connections between the domains are easy to estab-

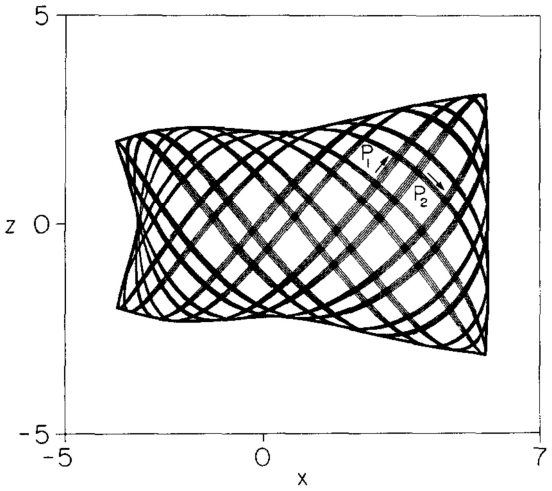

FIG. 1. The eigentrajectory for the coupled harmonic oscillator system. The caustics are also drawn.

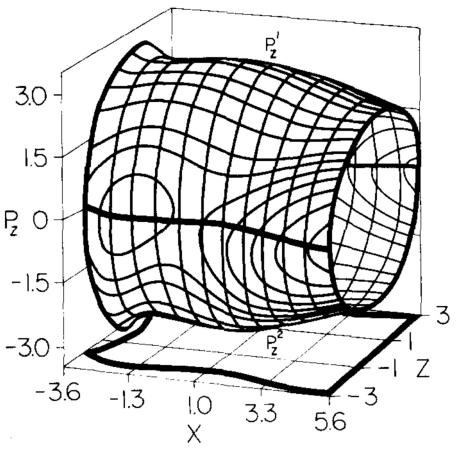

FIG. 2. The Lagrangian manifold as represented by $p_z(x,z)$ for domains 1 (upper portion of surface) and 2 (lower portion of surface). The caustic is outlined heavily in the base plane and on the surface. On the front surface trajectories pass from domain 2 to domain 1 at the negative z caustic; on the rear surface, trajectories pass from domain 1 to domain 2 at the positive z caustic. On the ends trajectories switch to or from domains 3 or 4, which form a surface similar to the one shown. Thus, a trajectory enters onto this surface from the left edge, and winds about it until it exits on the right.

TABLE I. Near the origin, a trajectory is assigned to a sheet based on the signs of the momenta. This procedure is unsatisfactory near the corners; to see this most easily, examine Fig. 1 near the midpoint of the left caustic. Near the corners, signs of mixed-space Jacobians times coordinates uniquely identify the sheet on which the trajectory lies.

	Away from corners		Near corners	
Sheet	p_x	p_z	$xJ(p_x,z)$	$zJ(x,p_z)$
1	+	+	−	−
2	+	−	+	−
3	−	−	+	+
4	−	+	−	+

lish. For example, a trajectory in domain 1 must eventually reach either the top or the right caustic; it then passes through the singular domain near that caustic and enters either domain 2 (if it hits the top) or domain 4 (right). These connections are important in the construction of the uniform terms, below. They also establish the connections between the sheets of the manifold. For example, along the lower caustic sheet 2 joins 1, while on the right 1 joins 4; these relations can be seen in Fig. 1.

C. Jacobian

The Jacobian is defined as

$$J(t) = \partial(x,z)/\partial(t,w^0). \tag{2.6}$$

The symbol w^0 requires explanation. The Jacobian represents the effect on the trajectory of a differential change in the initial conditions; in two dimensions the change in the initial conditions involves a single variable. Since the surface of section at $x = 0$ is available from the determination of the eigentrajectory, we used data from it to obtain initial conditions for a pair of trajectories spaced $\Delta z^0 = 0.01$ units apart in z. We thus actually integrated a pair of trajectories with initial coordinates given by $(0, -0.005)$ and $(0, +0.005)$. The differentiation with respect to w^0 in Eq. (2.9) is then approximated by a difference formula using the trajectory pair:

$$J(t) = (dx/dt)(\Delta z/\Delta z^0) - (\Delta x/\Delta z^0)(dz/dt), \tag{2.7}$$

where $\Delta x(\Delta z)$ is the difference between the $x(z)$ values on the adjacent trajectories. (A Jacobian has been generated in a different way by Gray, Child, and Noid[7] for Franck–Condon factors.)

Other Jacobians are also needed to calculate the wave function near caustics. These are mixed position and momentum space Jacobians, defined as

$$\tilde{J}_{p_x z} = \partial(p_x,z)/\partial(t,w^0), \tag{2.8}$$

$$\tilde{J}_{xp_x} = \partial(x,p_z)/\partial(t,w^0), \tag{2.9}$$

$$\tilde{J}_{p_x p_z} = \partial(p_x,p_z)/\partial(t,w^0). \tag{2.10}$$

The configuration space Jacobian, $J(t)$, Eq. (2.6), must be converted to four functions of configuration space variables $J_k(x,z)$, where $k = 1,...,4$ labels the four sheets of the manifold. It is therefore necessary to identify the sheet on which the trajectory is lying at all times t. For small $|x|$ or small $|z|$, we already mentioned that the signs of the momenta identify the sheets. Near the corners, the sheet can be assigned by comparing the signs of the mixed-space Jacobians. $J_{p_x z}$ has opposite signs near the right and left caustics, and J_{xp_z} has opposite signs near the upper and lower caustics. Hence, near the corners, the signs of $xJ_{p_x z}$ and zJ_{xp_z} identify the sheets. The assignments and labels are shown in Table I.

The functions $J_k(x,z)$ are related to $J(t)$ through the trajectory functions $x(t), z(t)$:

$$J_k(x(t),z(t)) = J(t). \tag{2.11}$$

This relationship gives the values of J on the points through which the trajectory passes, but we need $J_k(x,z)$ on a regular grid. To obtain these values, a grid of lines of constant z is established at intervals $z = 0.2$, and each time the trajectory crosses any of these grid lines the values of x, S, p_z, J, and the sheet number are recorded. After the trajectory has been recorded for a sufficiently long time, the data is interpolated in x at each fixed z to obtain a two-dimensional (x,z) grid with spacings (0.2×0.2). This interpolation is done separately for each domain. Two sheets of the resulting Jacobian functions $J_k(x,z)$ are shown in Fig. 3.

The absolute value of the inverse of a Jacobian represents a classical density.[8] As can be seen in Fig. 3, the Jacobians vanish at each caustic, so the classical density diverges there.

D. The characteristic function

The next step is to calculate the characteristic function S, which determines the phase of the primitive wave function.

Like J, S must be converted from a function of time, $S(t)$, to four functions of configuration space variables, $S_k(x,z)$. This is only possible if (1) $S(t)$ is obtained from an eigentrajectory, and (2) the Maslov phase corrections are incorporated into the definition of $S_K(x,z)$. Maslov [Ref. 1; see also Ref. 5(c)] has shown that the characteristic function is reduced by $\pi/2$ each time the trajectory switches sheets. For example, near the upper caustic ($z = z_c$), where trajectories on sheet 1 go to sheet 2, if $S_1(x,z_c) = S(t_c)$, then $S_2(x,z_c) = S(t_c) - \pi/2$. The procedure to convert to the functions incorporating these phase shifts is discussed next.

As already stated, $S(t)$ is recorded each time the trajectory passes through a z-grid line. On each individual z grid in each domain, the data is then arranged in order of increasing x. The trajectory winds through each domain in a complicated pattern, so points adjacent in x generally represent very different times, and $S(t)$ considered as a function of x on a grid line contains large discontinuities. We remove these discontinuities in S along a z grid by using the relationship $dS(x) = p_x dx$ to obtain a predicted value of $S(x)$:

$$S_{\text{pred}}(x_{n+1}) = S(x_n) + p_x(x_{n+1} - x_n)$$

and then a corrected value is obtained by subtracting the necessary multiple of $\pi/2$:

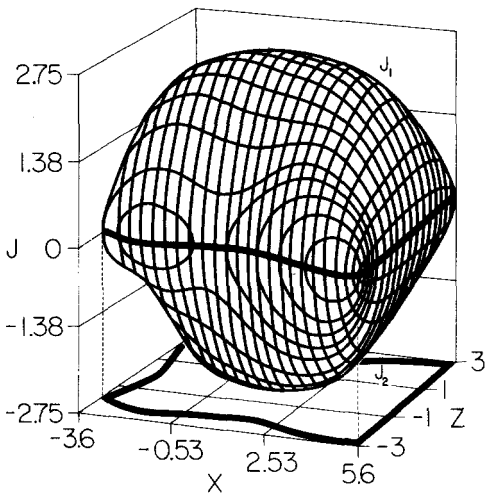

FIG. 3. The Jacobians $J_1(x,z)$ (upper portion of surface) and $J_2(x,z)$ (lower portion of surface), Eq. (2.10). The heavy line in the base plane and on the figure is the caustic, at which the Jacobians vanish.

$$m = [\{S(x_{n+1}) - S_{\text{pred}}\}/(\pi/2)], \quad m \text{ integer}, \tag{2.12}$$

$$S_k(x_{n+1}) = S(x_{n+1}) - m\pi/2. \tag{2.13}$$

This sequence of prediction and correction is continued all along the z-grid line and the whole process repeated for each grid line in each domain. At this point $S_k(x,z)$ is a smooth function of x on each z-grid line. After interpolation to obtain $S_k(x,z)$ on a regular grid in x, the procedure can be applied similarly to remove discontinuities in the z direction.

The final step is to establish the characteristic functions on sheets 2, 3, and 4 relative to sheet 1. We add an appropriate multiple of $\pi/2$ such that three Maslov phase conditions hold at caustics (modulo 2π):

$$\text{on the left:} \quad S_4(x_c,z) = S_1(x_c,z) + \pi/2, \tag{2.14}$$

$$\text{on the top:} \quad S_2(x,z_c) = S_1(x,z_c) - \pi/2, \tag{2.15}$$

$$\text{on the bottom:} \quad S_3(x,z_c) = S_4(x,z_c) + \pi/2. \tag{2.16}$$

Then all the other Maslov conditions are automatically satisfied because the eigentrajectory has half-integral quantization of action variables.

The resulting smooth characteristic functions are shown in Fig. 4. In domain 1, for example, the characteristic function increases in the direction of $+x$, $+z$, in accord with the relationship $\nabla S = p$. The connections between the S's on different domains are more difficult to see (because the Maslov phase shifts are built into these functions, and because of the presence of arbitrary differences of 2π), but careful examination will show that, for example, on the bottom caustic $S_1 = S_2 - \pi/2$.

III. WAVE FUNCTIONS

A. The primitive semiclassical wave function

The local asymptotic solution "to order $\hbar$" of the Schrödinger equation for regular domain k is shown in I to be given by

$$\Psi_k(x,z) = |J_k(x,z)|^{-1/2}\exp[iS_k(x,z)/\hbar]. \tag{3.1}$$

As shown in the previous section, the functions $S_k(x,z)$ implicitly contain the phase shifts associated with the Maslov indices. The full primitive semiclassical wave function at each point x,z is the sum of contributions associated with each regular domain that projects onto that point:

$$\Psi_p(x,z) = N\sum_k \Psi_k(x,z), \tag{3.2}$$

where N is a normalization constant.

A contour diagram and a projection of the primitive semiclassical wave function is shown in Fig. 5. The normalization constant N has been chosen so that the primitive semiclassical wave function agrees with the quantum mechanical wave function at $x = 3.2, z = 0.6$. The basic structure of the wave function is apparent; there are two interior nodes in the z direction and five in the x direction, as the quantum numbers for this state specify. The state also appears to be symmetric in z, as it must be according to quantum mechan-

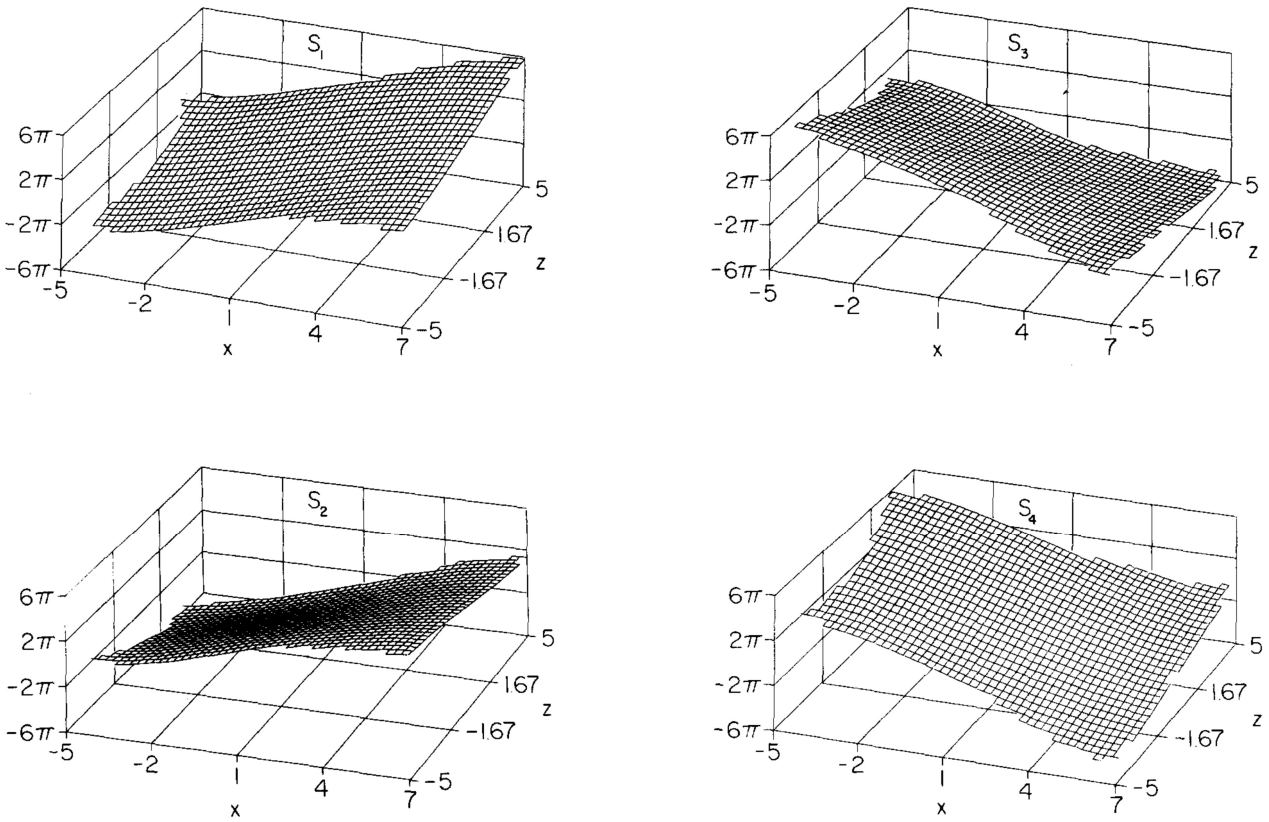

FIG. 4. The characteristic function $S_j(x,z)$, plotted separately for domains 1–4 in (a)–(d), respectively.

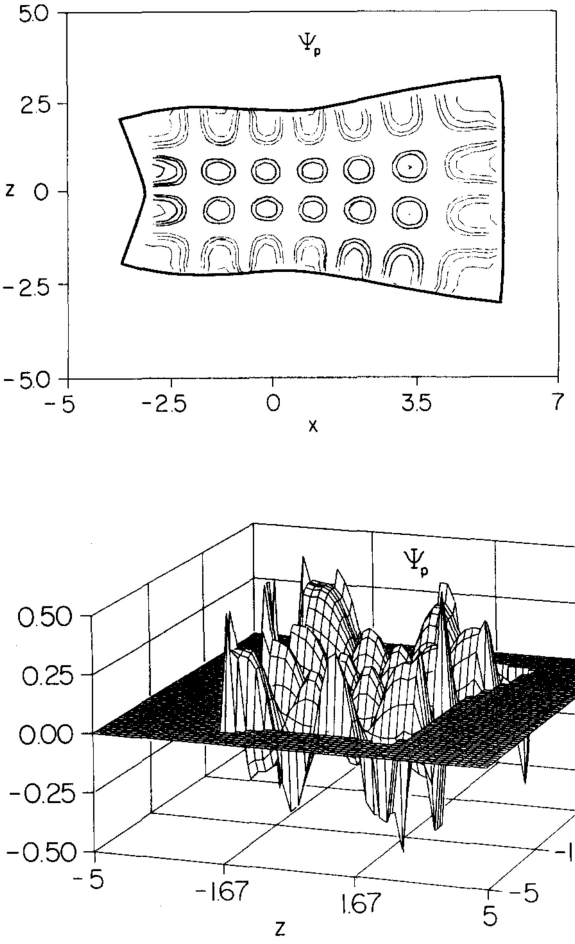

FIG. 5. The primitive semiclassical wave function $\Psi_p(x,z)$, Eq. (3.2). The wave function is artificially truncated close to the caustic, where the zero in the Jacobian causes the wave function to diverge. (a) Contour plot, contours at ± 0.10, ± 0.14, ± 0.20, ± 0.28, ± 0.40. The heavy line is the caustic. (b) Three-dimensional plot.

ics. Since the symmetry was not built into the computer code, this provides a good check of the accuracy of the procedure. The primitive semiclassical wave function diverges near the caustics, where the Jacobian $J(x,z)$ vanishes, and the plot has been artificially truncated to omit these points.

B. Uniform wave function

Near and outside of the caustics the primitive form is not suitable, and a uniform approximation is needed. We obtain a global wave function by combining a set of "transitional approximations," each of which is calculated by Fourier transformation of an appropriate mixed-space or momentum space form.

1. Edge functions

In the following we consider the transitional approximation appropriate in the singular domain adjacent to the upper (large z) caustic; the form for the bottom caustic is very similar, while those for the right and left sides are obtained by exchange of the roles of the x and z variables. The singular domain near the upper caustic has a smooth projection into the (x,p_z) space, and *in this space* a primitive wave function is suitable:

$$\tilde{\Psi}(x,p_z) = |\tilde{J}(x,p_z)|^{-1/2}\exp\{i\tilde{S}(x,p_z)/\hbar\}. \tag{3.3}$$

Then, as shown earlier (I), the leading term in the (inverse) Fourier transform of $\tilde{\Psi}(x,p_z)$ is

$$\Psi_{21}(x,z) = |2\pi/\tilde{J}_{21}(x)|^{1/2}b(x)\exp\{i\tilde{S}_{21}(z_c)/\hbar\} \times \mathrm{Ai}[\mathrm{sgn}(z_c)b(x)(z-z_c)], \tag{3.4}$$

where $z_c = z_c(x)$ is the position of the caustic, Ai is an Airy function, and $\tilde{J}_{21}$ is the mixed-space Jacobian $\tilde{J}_{p_x z}$, Eq. (2.7), evaluated at the caustic, $\tilde{J}_{p_x z}[x,p_z(x,z_c)]$. The subscript 21 indicates that this is the term which arises from trajectories changing to sheet 2 from sheet 1. The phase requires careful attention; at the caustic the outgoing phase is shifted from the incoming phase by $\pi/2$, so the edge phase has the form

$$S_{ji} = S_j + \pi/4 = S_i - \pi/4. \tag{3.5}$$

The quantity $b(x)$ has yet to be defined; the formal expression comes from the expression for the manifold in (x,p_z) coordinates, $z(x,p_z)$:

$$b(x) = |\{1/2[d^2z(x,p_z)/dp_z^2]\}|^{-1/3}. \tag{3.6}$$

However, because accurate numerical evaluation of the second derivative is difficult, we employ an approximate expression for this function. Near the caustic the trajectories are very nearly described by the uncoupled harmonic oscillator system obtained by setting the coupling constants k_{12} and k_{30} to zero. The trajectories then have analytic expressions and the caustic corresponds to the turning point, so we find under these conditions that

$$b(x) = |2k_z z_c|^{1/3}; \quad b(z) = |2k_x x_c|^{1/3}, \tag{3.7}$$

where we use the actual position of the caustic, not the uncoupled turning point, in the expression.

As the domains are connected in pairs along a caustic, there are two such terms on each edge; on top caustic, for instance, not only do trajectories labeled 1 make the transition to those labeled 2, generating a uniform term we labeled Ψ_{21}, but trajectories labeled 4 also join to those labeled 3, generating a Ψ_{34} term. Thus, the final edge function for the upper caustic is

$$\Psi_e(x,z) = \Psi_{21}(x,z) + \Psi_{34}(x,z), \tag{3.8}$$

Ψ_{21} differs from Ψ_{34} only in the characteristic function $S_{34} \neq S_{21}$. Formulas for wave functions along the other caustics are similar.

2. Corner functions

In the corners neither of the mixed-state representations provides an appropriate set for the manifold, and the fully momentum-space version with independent variables p_x, p_z must be used instead. From the semiclassical expression

$$\tilde{\Psi}(p_x,p_z) = |\tilde{J}(p_x,p_z)|^{-1/2}\exp\{i\tilde{S}(p_x,p_z)/\hbar\} \tag{3.9}$$

a Fourier transform in both variables gives the configuration space wave function. An additional approximation (Appendix) leads to an expression of the form

$$\Psi_I(x,z) = C_I\,\mathrm{Ai}[\mathrm{sgn}(x_c)b(z)(x-x_c)] \times \mathrm{Ai}[\mathrm{sgn}(z_c)b(x)(z-z_c)], \tag{3.10}$$

where C_I is a complex constant, x_c and z_c are the positions of the caustics or their extensions into the forbidden region, and the subscript I labels the corner. The constants may be evaluated by requiring the corner function to match the edge function at a position where their domains overlap; a convenient choice is on one of the caustics. Thus the condition determining C_I is

$$\Psi_I(x_c,z) = C_I \,\mathrm{Ai}[0]\mathrm{Ai}[\mathrm{sgn}(z_c)b(x)(z-z_c)] = \Psi_e(x_c,z). \tag{3.11}$$

3. Semiclassical wave function

The total global semiclassical wave function is given by the sum of all of the above terms combined by switching functions. These switching functions confine the influence of a given term to the domain for which it is appropriate (recall that domains overlap). For convenience we use a single type of switching function

$$e_x(xz) = 0.5(1+\tanh\{(2.8/o) \times [x - x_c(z) + \mathrm{sgn}(x_c)*o]\}), \tag{3.12}$$

$$e_z(zx) = 0.5(1+\tanh\{(2.8/o) \times [z - z_c(x) + \mathrm{sgn}(z_c)*o]\}), \tag{3.13}$$

where o, an offset from the caustic, is 0.85 for e_x and 0.60 for e_z, and e_z is used for the upper and lower caustics, e_x, on the left and the right. This switching function vanishes well inside a caustic, reaches 0.5 at the distance o inside the caustic, and is greater than 0.99 at and beyond the caustic.

At any point (x,z) the nearest edge term is combined wtih the closest corner

$$\Psi_u(x,z) = (1 - e_x e_z)\Psi_e + e_x e_z \Psi_I \tag{3.14}$$

and this is combined with the primitive wave function to obtain the final expression for the complete wave function:

$$\Psi(x,z) = [1 - e_v(x,z)]\Psi_p(x,z) + e_v(x,z)\Psi_u(x,z), \tag{3.15}$$

where v is the coordinate nearly perpendicular to the nearest caustic.

IV. RESULTS

The magnitude of the resulting wave function is shown with both a contour plot and a three-dimensional representation in Fig. 6. The semiclassical wave function is fit to the quantum variational function at a single point, just as was the primitive semiclassical wave function. The caustic is superimposed as a heavy line on the contour plot. The effect of the Airy-function transitional terms can be seen along each caustic and in the corners, where they smoothly join on to the primitive functions. The Airy-function forms are well behaved near the caustics, and they decrease exponentially in the forbidden region.

For purposes of comparison, we have also determined a fully quantum wave function of the form

$$\Psi_q(x,z) = \sum_{n_x,n_z} c_{n_x n_z} u_{n_x}(x) u_{n_z}(z), \tag{4.1}$$

where the u's are harmonic oscillator functions with appropriate force constants. We used a 300 state basis [25 $u_n(x)$ $\times$ 12 odd-parity $u_n(z)$] to obtain the function plotted in contour and three-dimensional form in Fig. 7. The classical caustics are also superimposed on the contour diagram as a heavy line, and provide an outer boundary for the quantum wave function. The three-dimensional plot shows the semiclassical and quantal functions to be in good agreement, with an identical pattern for the two functions. The contour diagram shows the degree of quantitative agreement to be high, with the corner regions showing the largest deviations. This deviation probably arises from the "near-separable" approximation we used in that region (Appendix).

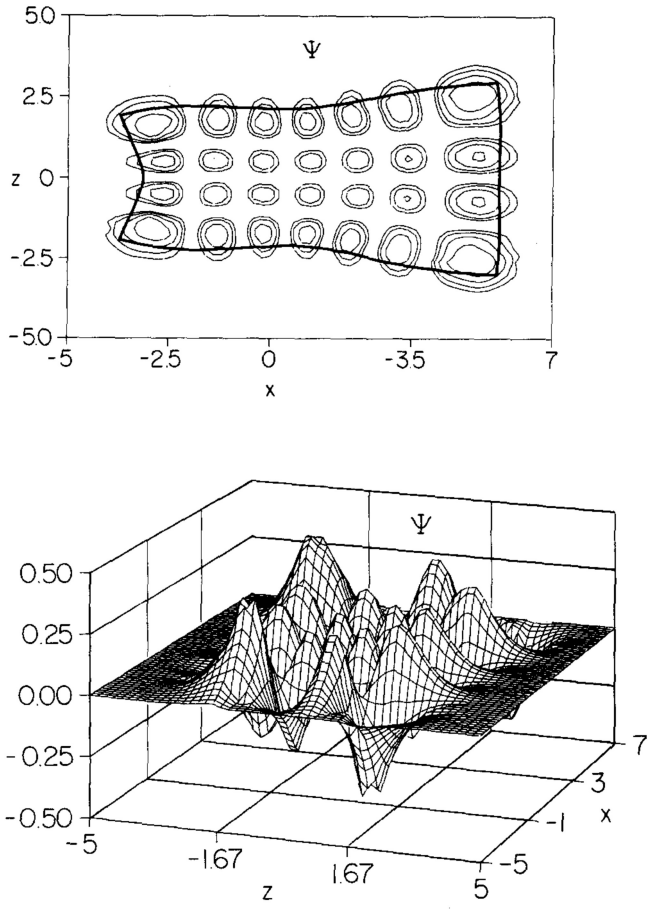

FIG. 6. The semiclassical wave function $\Psi(x,z)$, Eq. (3.15). (a) Contour plot, contours at ± 0.10, ± 0.14, ± 0.20, ± 0.28, ± 0.40. The heavy line is the caustic. (b) Three-dimensional plot.

The global picture presented in Figs. 6 and 7 is supplemented by the detailed comparisons shown in Fig. 8, in which slices of the semiclassical and quantal wave functions at fixed x or z are plotted as functions of z or x, respectively. The quantitative agreement is seen to be excellent, with the wave functions practically indistinguishable except near and outside the caustics. In Fig. 8(a), a slice at $x = -1.4$ a.u., the primitive and semiclassical wave functions are of virtually identical up to the caustics, where the singularity in the primitive function is clearly seen. The primitive function provides an excellent representation of the wave function to within about 0.5 units from the caustic, confirming that the improper behavior is restricted to a narrow region. The tran-

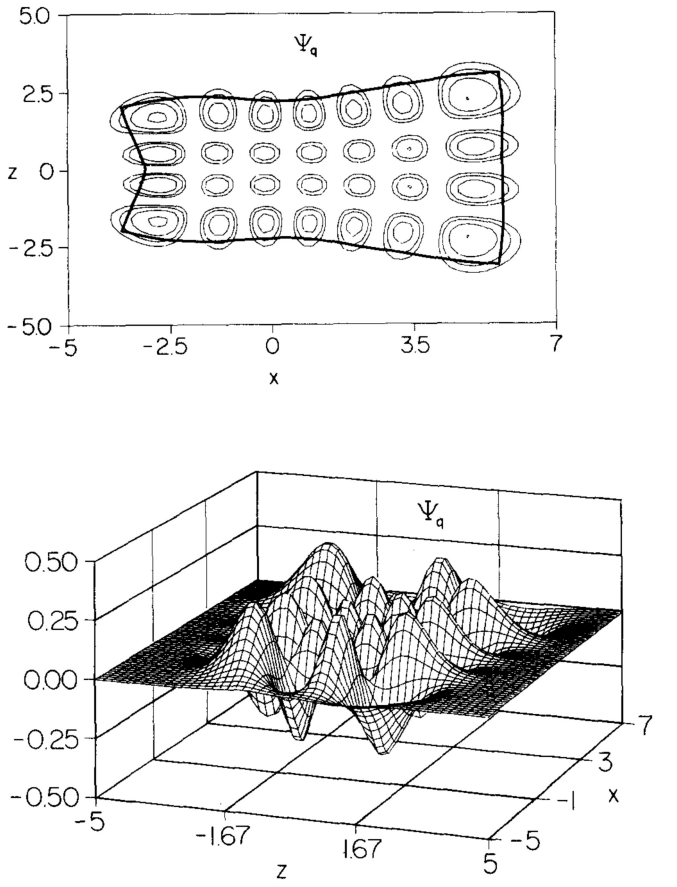

FIG. 7. The semiclassical wave function $\Psi_q(x,z)$, Eq. (4.1). (a) Contour plot, contours at ± 0.10, ± 0.14, ± 0.20, ± 0.28, ± 0.40. The heavy line is the caustic. (b) Three-dimensional plot.

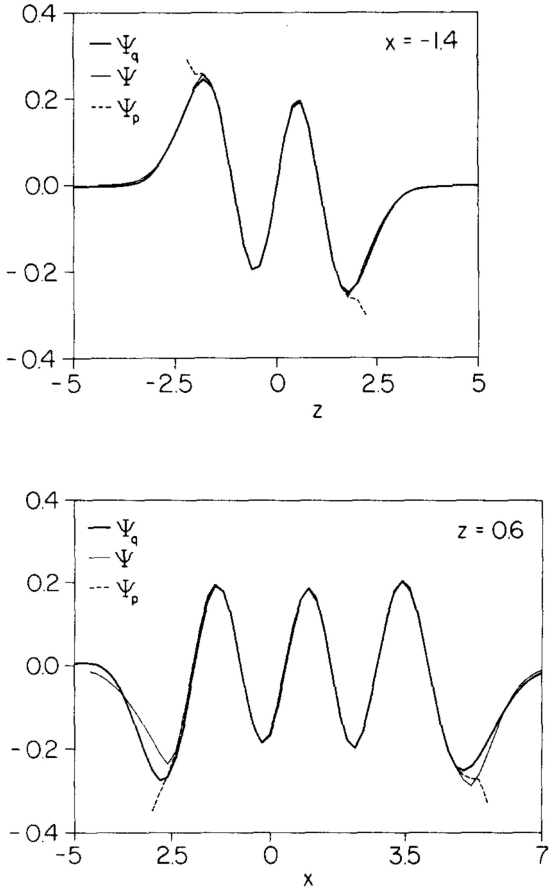

FIG. 8. Slices of primitive (dashed line), semiclassical (light solid line), and quantum (heavy solid line) wave functions. (a) $x = -1.4$, (b) $z = 0.6$.

sitional Airy-function approximation provides an excellent representation near and beyond the caustic. In Fig. 8(b), a slice at $z = 0.6$, the behavior is seen to be similar, except that the transitional term is not quite as accurate, probably because the approximation for b [Eq. (3.7)] is not as good in this case.

In order to examine the influence of the Jacobian on the wave function, we also define a simple type of primitive semiclassical wave function in which it is omitted:

$$\Psi_s = N' \sum_k \exp(iS_k/\hbar), \tag{4.2}$$

where N' is chosen to match this function to the quantum wave function at $x = 3.2$, $z = 0.6$. (We repeat that the Maslov phase shifts are implicitly included in our definition of S.) Slices of this function and the quantum wave function are plotted in Figs. 9(a) and 9(b). By omitting J, the catastrophe at the caustic is avoided. The curvature (but not the magnitude) of the wave function at the caustic closely follows the quantum function, indicating that the phases are accurate near the caustic; this was also indicated by the proper nodal structure of the semiclassical wave function along the caustics. However, the magnitude of this zero-order primitive wave function is not in good agreement with the quantum results until well inside the caustic ($|z - z_c| > 1$), where the Jacobian is relatively flat; the standard primitive wave function provides a better approximation over a larger range of the variables.

A number of numerical tests of the accuracy of the semiclassical wave function have also been conducted. The symmetry of the system implies that $J_1 = J_3$, $J_2 = J_4$, $p_{z1} = -p_{z2}$, and $p_{z3} = -p_{z4}$; generally these conditions are satisfied to more than five-digit accuracy even after interpolation to the regular grid in x. The other tests concern the wave function itself. As mentioned earlier, we multiplied the semiclassical wave function by a constant so that it would exactly match the normalized quantum wave function at one point. Hence the norm of the semiclassical wave function provides a test of its global accuracy. The norm is

$$O_{sc} = \int |\Psi_{sc}(x,z)|^2 dx\, dz. \tag{4.3}$$

Numerical evaluation of this integral by the trapezoidal rule, using only values at the grid points, gives $O_{sc} = 1.24$ with the scaling as described above. There are two primary sources for the error in O_{sc}: (i) the numerical error in the integration on this fairly wide grid, which we estimate at about 4%, and (ii) the visible error in the transitional approximations in the corners. We have also calculated the overlap of the semiclassical with the quantum wave function using the same numerical integration procedure and obtained 0.98

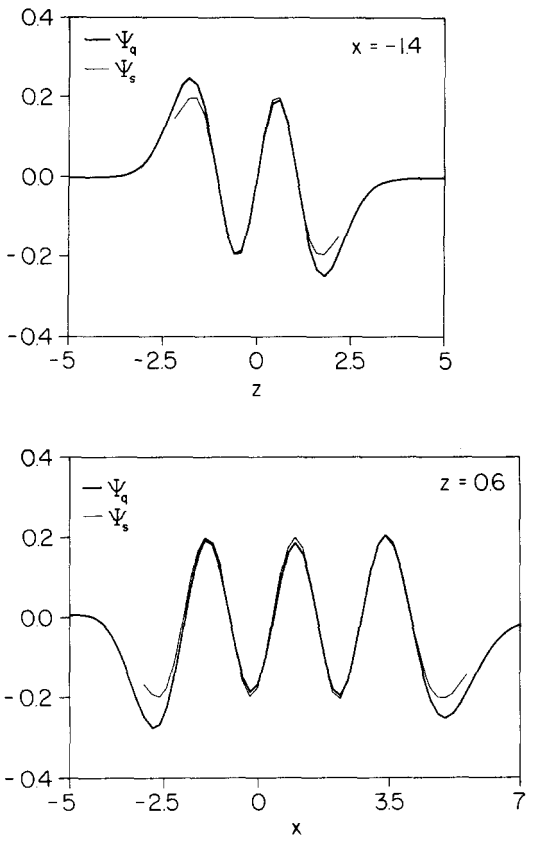

FIG. 9. Slices of the simple primitive (light) and quantum (heavy) wave functions. (a) $x = -1.4$, (b) $z = 0.6$.

$(O_{sc} \times O_q)^{1/2}$, demonstrating a very high overlap between the approximate and exact functions.

A final stringent numerical test involves the calculation of the overlap of the semiclassical function with the harmonic oscillator basis functions

$$d_{n_x n_z} = \int \Psi_{sc}(x,z) u_{n_x}(x) u_{n_z}(z) dx\, dz / \sqrt{O_{sc}} \qquad (4.4)$$

and the comparison of these coefficients with corresponding coefficients for the exact quantum wave function

$$c_{n_x n_z} = \int \Psi_q(x,z) u_{n_x}(x) u_{n_z}(z) dx\, dz. \qquad (4.5)$$

The results for the 15 basis functions with the largest coefficients in the quantum wave function are listed in Table II. These 15 terms constitute 92% of the wave function in the sense that $\Sigma d^2_{n_x n_z} = 0.92$. In the table the x and z quantum numbers are listed in the second and third columns, respectively, followed by the quantum $c_{n_x n_z}$ and semiclassical $d_{n_x n_z}$ coefficients in the fourth and fifth columns. Generally the coefficients agree within 10% or better.

TABLE II. Columns 2 and 3 specify the x and z quantum numbers. Column 4 contains the 15 coefficients of largest magnitude in the (25×12) state quantum variational calculation of the eigenstates, in order of decreasing magnitude. The fifth column is the coefficient as obtained by integration of the semiclassical function with the harmonic oscillator basis function, Eq. (5.3).

k	n_x	n_z	$c_{n_x n_z}$	$d_{n_x n_z}$
1	5	3	−0.483	−0.480
2	4	3	0.427	0.408
3	8	3	0.347	0.345
4	9	3	0.293	0.295
5	6	3	−0.255	−0.223
6	7	3	0.241	0.222
7	10	3	0.211	0.216
8	8	5	0.149	0.197
9	9	5	0.149	0.173
10	11	3	0.138	0.153
11	10	1	−0.137	−0.153
12	3	3	−0.135	−0.139
13	10	5	0.120	0.154
14	9	1	−0.116	−0.082
15	4	5	−0.110	−0.105

V. CONCLUSIONS

The mathematical developments in multidimensional semiclassical theory have been applied to the computation of a bound-state wave function. The method is practical and leads to a wave function which is an accurate representation of this excited state.

APPENDIX: WAVE FUNCTIONS NEAR THE CORNERS

A more complete discussion of wave functions near the corners will be given in a future article. Here we give a brief outline of the arguments leading to Eq. (3.10). Near the corners, the Lagrangian manifold has a smooth, invertible projection into p_x, p_z space, and it has a generator $\tilde{S}(p_x,p_z)$. This generator must satisfy the Hamilton–Jacobi equation in momentum space,

$$(p_x^2 + p_z^2)/(2M) + V(-\partial S/\partial p_x, -\partial S/\partial p_z) - E = 0. \qquad (A1)$$

If $\tilde{S}(p_x,p_z)$ is expanded in a Taylor series about $p_x = 0$, $p_z = 0$, one finds from Eq. (A1) that S has linear and cubic terms in the p's, but no quadratic terms: to degree 3, S is given by

$$\tilde{S}(p_x,p_z) = \tilde{S}(0,0) - (p_x x^0 + p_z z^0) + (1/3)Ap_x^3 + (1/2)Bp_x^2 p_z + (1/2)Cp_x p_z^2 + (1/3)Dp_z^3 + \cdots, \qquad (A2)$$

where x^0, z^0 represent the position of the corner, and A–D are constants which must be chosen such that Eq. (A2) satisfies Eq. (A1).

The arguments that are used by catastrophe theorists[9] tell us that there is a point transformation among the P's,

$$P_1 = P_1(p_x,p_z),$$
$$P_2 = P_2(p_x,p_z) \qquad (A3)$$

such that $\tilde{S}$ can be written *exactly* as

$$\tilde{S}(P_1,P_2) = (1/3)aP_1^3 + (1/3)aP_2^3 - Q_1^0 P_1 - Q_2^0 P_2. \qquad (A4)$$

This generator corresponds to a special case of the so-called Hyperbolic Umbilic catastrophe. (The canonical form for the generator of this catastrophe also contains a term cP_1P_2, but it can be shown that the term vanishes in the present case.)

Corresponding to the point transformation [Eq. (A3)] among P's, there is a point transformation among Q's,

$$Q_1 = Q_1(x,z),$$
$$Q_2 = Q_2(x,z), \tag{A5}$$

such that the complete transformation $(p_x,p_z,x,z) \rightarrow (P_1, P_2, Q_1, Q_2)$ is canonical. In these coordinates, the Lagrangian manifold is described by the equations

$$Q_1(P_1,P_2) = -\partial S/\partial P_1 = Q_1^0 - aP_1^2,$$
$$Q_2(P_1,P_2) = -\partial S/\partial P_2 = Q_2^0 - bP_2^2. \tag{A6}$$

Singular points of this manifold are the lines $Q_1 = 0, Q_2 = 0$. It can be shown that these singular points correspond to two curves in xz space that meet in a right angle at the corner.

In these new coordinates, the semiclassical approximation to the wave function in P space is

$$\tilde{\Psi}(P_1,P_2) = |\tilde{J}(P_1,P_2)|^{-1/2} \exp[i\tilde{S}(P_1,P_2)/\hbar] \tag{A7}$$

and the corresponding wave function in Q space is

$$\Psi(Q_1,Q_2) = (-2\pi ih)^2 \int \exp[i(P_1Q_1 + P_2Q_2)/\hbar] \times \tilde{\Psi}(P_1,P_2)\,dP_1\,dP_2. \tag{A8}$$

When the form (A4) is put into Eq. (A8), and the approximation that $J(P_1,P_2)$ be constant is used, the integral is separable, and one arrives immediately at the result that $\Psi(Q_1,Q_2)$ is a product of Airy functions.

This means that near the corners, there exist orthogonal coordinates $Q_1(x,z)$ $Q_2(x,z)$ such that the two curves $Q_1(x,z) = Q_1^0$ and $Q_2(x,z) = Q_2^0$ correspond to the two caustics. In these coordinates, the semiclassical wave function can be written as a product of Airy functions:

$$\Psi(Q_1,Q_2) = c\,\mathrm{Ai}[\alpha_1(Q_1 - Q_1^0)]\mathrm{Ai}[\alpha_2(Q_2 - Q_2^0)]. \tag{A9}$$

In principle, the constants c, α_1, and α_2 can be obtained from the constants a and b in Eq. (A4), which in turn are related to the constants A–D in Eq. (A2). However, it is more convenient to determine the constants approximately by comparison of the corner functions with the previously determined edge functions.

Finally, for the state considered here, the perpendicular lines defining the corner are close enough to (x,z) coordinates that for our purposes we can use the approximation

$$\Psi = c\,\mathrm{Ai}\{b_z(z)[x - x^0(z)]\}\mathrm{Ai}\{b_x(x)[z - z^0(x)]\}. \tag{A10}$$

ACKNOWLEDGMENTS

JBD acknowledges a grant from the National Science Foundation. SKK and JBD acknowledge support from the Kate and Thomas Jeffress Memorial Trust. DWN acknowledges support from the U.S. Department of Energy. Acknowledgment is made to the donors of the Petroleum Research Fund, administered by the American Chemical Society, for the partial support of this research. We thank L. Menges for many of the drawings.

[1] M. Fedoriuk and V. P. Maslov, *Semiclassical Approximation in Quantum Mechanics* (Reidel, Boston, 1981).
[2] J. B. Delos, Adv. Chem. Phys. **65**, 161 (1986); J. B. Delos, S. K. Knudson, and B. Bloom, J. Chem. Phys. **83**, 5703 (1985).
[3] Recently, wave functions have been calculated by other methods; M. J. Davis and E. J. Heller, J. Chem. Phys. **75**, 3916 (1981); N. De Leon and E. J. Heller, *ibid.* **78**, 4005 (1983); J. Ozment, D. T. Chuljian, and J. Simons, *ibid.* **82**, 4199 (1985).
[4] (a) J. B. Delos and R. T. Swimm, Chem. Phys. Lett. **47**, 76 (1977); (b) R. T. Swimm and J. B. Delos, J. Chem. Phys. **71**, 1706 (1979); (c) D. W. Noid, M. L. Koszykowski, and R. A. Marcus, Annu. Rev. Phys. Chem. **32**, 267 (1980).
[5] (a) A. Einstein, Verh. Dtsch. Phys. Ges. **19**, 82 (1917); (b) L. Brillouin, J. Phys. **7**, 353 (1926); (c) J. B. Keller, Ann. Phys. (NY) **4**, 180 (1958); (d) R. A. Marcus, Faraday Discuss. Chem. Soc. **55**, 34 (1973).
[6] D. W. Noid and R. A. Marcus, J. Chem. Phys. **62**, 2119 (1975); **67**, 559 (1977).
[7] S. K. Gray, M. S. Child, and D. W. Noid, Mol. Phys. **54**, 573 (1985).
[8] L. Pauling and E. B. Wilson, Jr., *Introduction to Quantum Chemistry* (McGraw-Hill, New York, 1935), p. 76.
[9] T. Poston and I. Stewart, *Catastrophe Theory and its Applications* (Pitman, London, 1978).